Laser-Pulse Melting of Nuclear Refractory Ceramics[1]

C. Ronchi[2, 3] and M. Sheindlin[2]

An accurate method for melting-point measurement of refractory nuclear ceramics was developed, based on laser-pulse heating and thermal arrest detection. The temperature measurement is performed by a combined use of a brightness pyrometer and a high-speed spectrometer working in the range of 500 to 900 nm. This method provides both the true temperature and the spectral emissivity function of the examined materials. Pure sintered MgO and a Mg:Am mixed oxide were first measured. The resulting melting point of the former (2350 ± 20 K) is significantly higher than that commonly recommended and decreases with the addition of americium. Furthermore, UO_2 irradiated to 37,000 MWd/t and submitted to a reactor loss-of-coolant test was investigated: the melting point decreases from 3120 K, in the as-fabricated state, to 2950 K. Both fresh Zr:U mixed oxides and ''corium'' lava from a reactor meltdown experiment were also investigated.

KEY WORDS: americium; corium; magnesium oxide; melting point; multi-channel pyrometry; reactor-irradiated uranium dioxide; zirconium oxide.

1. INTRODUCTION

In several aspects, the safe performance of nuclear reactors relies on the high melting point of the fuel. In this perspective, not only are refractory ceramics consisting of uranium and plutonium compounds continuously tested, but also inert matrices in which dispersed phases of highly radio-toxic actinides are burned through nuclear reactions. Moreover, during hypothetical severe accidents where the various core components may interact at high temperatures, ceramic compounds, mostly mixed oxides, represent the principal reaction products. Also, in this case, the melting

point of these reaction products is a crucial parameter on which the eventual extent of core meltdown depends. Therefore, work is still in progress to characterize the melting behavior of a number of ceramics present in nuclear reactors. Actually, despite the progress made in high-temperature measurements, there is still great discrepancy in the literature melting data, even for common and widely used materials. This is due in part to the fact that, in conventional furnace melting, perturbations are created by chemical instability of the compounds or reactions with the crucible.

On the other hand, however, although the application of laser heating methods makes it possible to produce melting under very clean conditions, serious disturbances still contribute to producing a loss of accuracy in the melting-point determination, i.e., (a) the relatively high vaporization rate of most ceramic oxides at the melting temperature produces a layer of aerosols that absorbs thermal radiation; (b) sample cracking due to low thermal shock resistance causes difficulties in controlling the heat exchange of the surface layer with the surroundings, resulting in unstable pyrometric measurements; (c) the unknown, mostly variable thermooptical properties in the vicinity of the melting point make the conversion of brightness to true temperature unreliable and problematic; and (d) moreover, since data are demanded for these materials not only in the as-fabricated state, but also after long residence times in the reactor, additional handling difficulties are faced due to the high radioactivity of the samples. The method and the experimental setup developed in this work are intended to reduce the above-mentioned difficulties substantially and provide accurate measurements of refractory nuclear materials. Two problems are examined in this paper. The first regards the use of magnesia as an inert matrix in which dispersed americium is ''burned'' by neutrons. The second deals with the melting behavior of zirconia–urania mixed oxides as reaction products of irradiated uranium dioxide fuel with oxidized zircalloy.

2. EXPERIMENTAL

2.1. Heating

The sample is housed in a small cylindrical vessel provided with an optical window, through which both heating and pyrometric measurements are performed. The sample is held by three zirconia pins or mounted in a metallic cylindrical holder of 25 mm diameter, where the space between the holder and the specimen is filled with cement glue. The vessel is equipped with two gas connectors, which enable the internal volume to be rinsed with inert gas. Since some of the examined samples were highly γ-radioactive, a second, *ad hoc* shielded device was constructed and assembled for
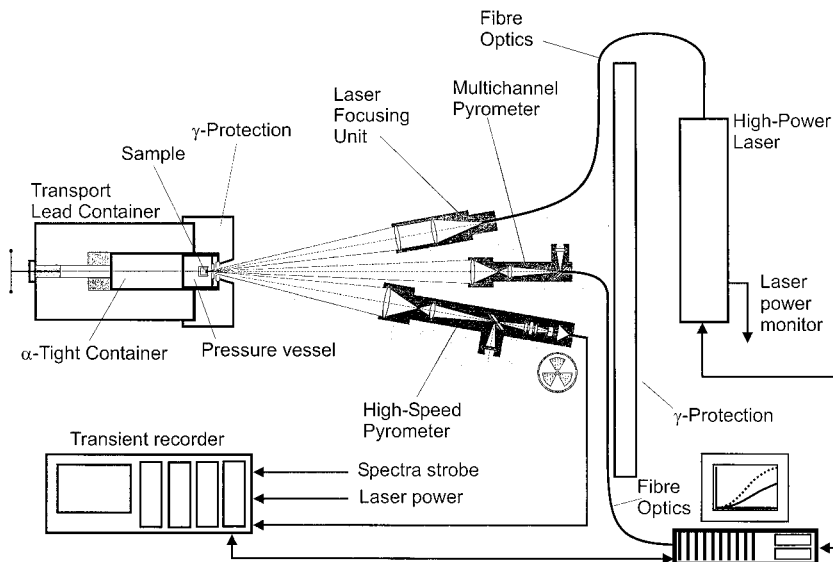
Fig. 1. Schematic of the setup.

the reported melting experiments. In this setup, the sample vessel is placed in the stainless-steel container of a standard lead-shielded transporting device. Fig. 1 shows a schematic of the apparatus.

Heating was provided by a medium-power (350-W) YAG:CW laser. A computer-controlled, arbitrary-function generator was used to drive the laser power supply, with a time resolution of 1 ms. The laser radiation was transferred to the optical bench of the setup through a fiber, and was conveyed on the sample surface by a focusing system. This produces a focal spot 4 to 5 mm in diameter with a very homogeneous power distribution. Self-crucible melting was realized by long (several seconds) controlled laser pulses. The time profile of the pulse was programmed according to the properties of the substance (expected melting temperature, light absorbency, heat conductivity, and thermal shock resistance) to reach a peak temperature above the melting point without producing significant axial thermal gradients, and by minimizing the risk of crack formation. At the end of the heating ramp, when the conditioning temperature attains a value of 300 to 400 K above the melting point, the power is decreased to a stationary level corresponding to approximately 50 to 70% of the maximum. Computer code simulation of these melting experiments shows that decreasing the power to this level—instead of completely switching off the laser—leads, during cooldown, to a significant increase in the duration of

the solidification plateau, as well as to a greater temperature stability. In fact, experimental tests confirmed that (1) undercooling during solidification can be effectively eliminated and (2) the phase-transition plateau lasts more than 100 to 200 ms, a relatively long time in this context.

In practice, a rather complex power-vs-time profile is first programmed and applied to ensure smooth heating of the sample up to the maximum temperature. The power is then submitted to a sharp decrease to the lower level, and cooling starts with a surface temperature rate of the order of 10,000 $K \cdot s^{-1}$. The onset of thermal arrest at the freezing temperature normally results in a pronounced knee in the cooling curve. For compounds of variable stoichiometry, model calculations indicate that at these cooling rates the temperature at the end of the thermal arrest plateau is very near to the solidus (actually, an analysis of the slope of the thermal arrest plateau may furnish information on the liquidus/solidus gap; this analysis is, however, not sufficiently precise at these high cooling rates).

2.2. Pyrometric Method

A monochromatic pyrometer and a fast spectrometer simultaneously perform temperature measurements. The first one is a fast (10-μs-rise time) monochromatic brightness pyrometer (650 ± 10-nm wavelength, 0.7-mm sighting spot). This pyrometer operates with a Si detector connected to a very precise log-amplifier and *14-bit* precision transient digitizer. The pyrometer was repeatedly calibrated for *brightness* temperature above 2400 K with certified tungsten-strip lamps. The correction for the presence of the double window of the vessel was made by spectral absorbence measurements of the window with a standard spectrophotometer. A high-speed spectropyrometer (0.3-mm spot size) is used simultaneously to obtain a proper evaluation of the *true* temperature. This covers the wavelength range of 500 to 900 nm; the measured spectrum consists of 200 points, which are recorded in about 4 ms. The buffer of the spectropyrometer enables one to record 32 spectra in 120 ms, with an integration time sufficiently long for the Si array to produce a usable signal. The start of recording is normally synchronized with the onset of the freezing process.

The absolute calibration of the spectropyrometer was made against a tungsten-strip lamp and a high-temperature blackbody (BB) model. In this kind of application, the most important requirement for the spectrometer is good linearity. This was investigated by using a stable light source (tungsten-strip lamp) and by varying the integrating time of the diode array. Since the main source of non-linearity is the current-to-voltage conversion, an increase in the integration time with a constant light intensity simulates the increase in light intensity. Actually, the response of all 200

diodes of the array was found to be noticeably nonlinear. Since, however, the deviation from non-linearity could be easily compensated with a simple parabolic function, this correction was automatically applied to the primary data. After that, the non-linearity deviations of the photodiode response became negligibly low ($<0.2\%$). An *absolute* intensity calibration at the wavelength of 650 nm was carried out against a tungsten-strip lamp. The extension of the calibration to the whole spectral range of 500 to 900 nm was made by means of a source of high-temperature BB radiation. This calibration was repeated at several temperatures up to 3200 K. A proof of the adequacy of the BB calibration is that the measured sensitivity curve, defined by

$$S(T, \lambda) = J_{\text{counts}}(T, \lambda)/I_{\text{Plank}}(T, \lambda)$$

does *not* depend on the BB temperature. Since the linearity of the system was checked independently, the ratios of the sensitivities taken at different temperatures confirm that, in the examined wavelength range, the spectral radiance distribution of the BB source does not depend on the temperature. It should be noted that no type of direct measurement could prove the self-consistency of the BB model. Finally, the following hybrid procedure was adopted for the true temperature evaluation: (a) the brightness temperature was measured with the high-precision and high-speed monochromatic pyrometer; (b) analysis of the thermal spectrum (an extension of that described in Ref. 1) was performed to deduce the spectral emissivity function, $\varepsilon = \varepsilon(\lambda)$, and a previous evaluation of the true temperature (with a precision of approximately 0.2%); and (c) the final true temperature was calculated from a, by using the emissivity at 650 nm obtained in b, with a precision of the order of 0.1%.

3. MELTING-POINT MEASUREMENTS

3.1. MgO

The samples were fabricated in our ceramic laboratory in the form of sintered pellets of 6-mm diameter and 8-mm length, from a high-purity powder (<400 ppm impurities). The targeted sintered density was rather low (85% of the theoretical density value), to ensure better resistance of the pellets to thermal shocks. The pellets are white at room temperature and do not change in color after repeated melting under inert gas. Heating by laser irradiation is, therefore, difficult, however, as for most semitransparent ceramic oxides, absorption in the visible and near-IR spectral range increases with temperature.
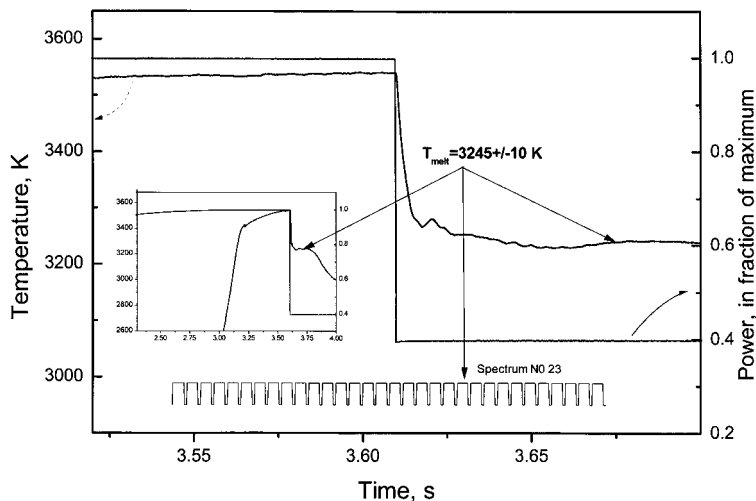
Fig. 2. Laser-power profile and thermogram showing thermal arrest during MgO freezing.

A thermogram of a MgO melting test is shown in Fig. 2; the inset is a plot of the solidification plateau with the position of the spectra recorded during the phase transition. The deduced spectral emissivity curves are shown in Fig. 3. In the selected wavelength interval, the *effective* emissivity of the liquid is between 0.95 and 1, while during solidification it decreases to 0.92 ± 0.1. The spectral emissivity at the melting point appears to be effectively constant (only two absorption peaks due to alkali impurities in the vapor are detected), except in the lowest-wavelength segment, where a decrease in $\varepsilon(\lambda)$ is observed. The evaluation of the true-temperature accuracy depends principally on two related experimental conditions: the actual transparency of the sample and the existence of positive thermal gradients between the sample surface and the underlying layer. Experiments were therefore carried out at different cooling rates, producing larger axial gradients. It was observed that the effective emissivity at the freezing point increases with the cooling rate, revealing a contribution of hotter internal layers to the measured spectrum. By varying the cooling rates below a sufficiently low value, the effective emissivity remains constant. Obviously, this does not exclude bulk contribution effects, however, the correctness of the measurement is corroborated by the coinciding temperature values obtained from the spectral analysis (based on *fractional* spectral intensities) and from the *absolute* signal of the brightness pyrometer. The solidification point was finally determined at 3250 ± 20 K.
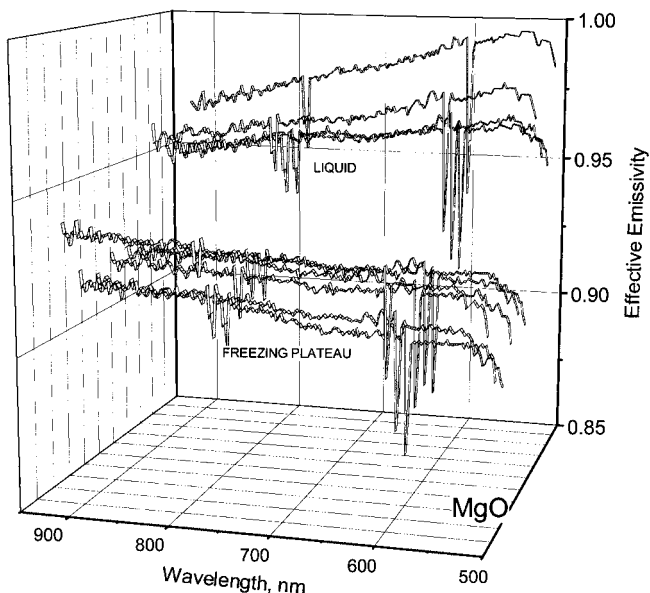
Fig. 3. Effective spectral emissivity of MgO during freezing and just above the melting point. The sharp absorption wells are due to alkali impurities in the surrounding atmosphere.

A mixed oxide, MgO:1.5 at% AmO_2, was then measured. This oxide, also in the form of high-density sintered pellets, is dark-gray colored. Since sintering started from a mechanically blended powder, a preliminary laser pulse was applied, after which americium was homogeneously dissolved in the molten region. This appeared black at visual inspection: actually, a high emissivity was measured ($\varepsilon_{600\,nm} = 0.78$), which corresponds to the *real* spectral emissivity, for the optical transmittance of this mixed oxide is negligible.

In Fig. 4 are plotted the thermograms of two pulses with the respective laser power histories: the first one (2), reaching approximately 3100 K, does *not* exhibit any freezing plateau, while the other (1), peaking at 3500 K, shows a clear recalescence plateau at 3220 K. This temperature corresponds to the solidus point of the sample within a precision of approximately ± 15 K. The scatter in the freezing point obtained from measurements of three samples was of the same order of magnitude. The accuracy of the true pyrometric temperature here is better than in the case of the white, translucid MgO. The measured melting point of MgO ($T_m = 3250 \pm 20$ K) is significantly higher than that customarily assumed (3100 K). By considering the melting production and detection method adopted, as well as the quality of the pyrometers used in this work, an error of 150 K in T_m can
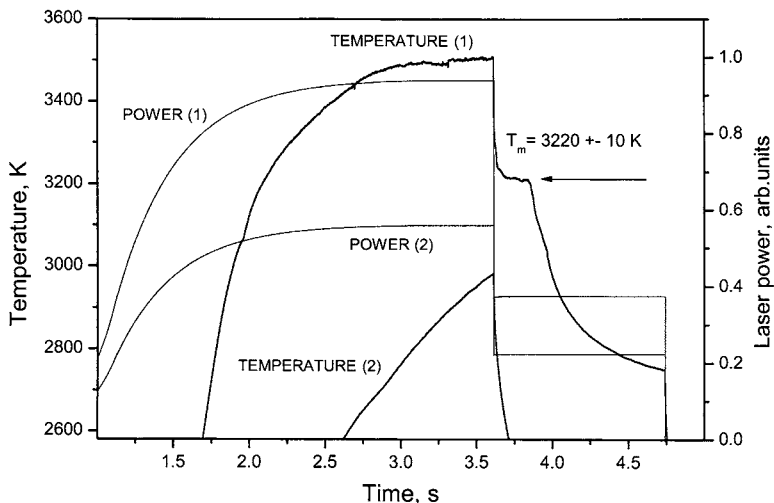
Fig. 4. Effect of two consequent pulses applied to americium-doped magnesia. While pulse 1 produces a clear thermal arrest at 3220 K, pulse 2, with a maximum temperature just below 3000 K, does not produce melting.

certainly be excluded. We must, therefore, conclude that the previous measurements were suspect.

Actually, alternative classical melting experiments on MgO produce relevant sources of errors, the major of which is probably caused by the high equilibrium vapor pressure of this oxide (the boiling point is just above the melting temperature), accompanied by chemical dissociation processes. Furthermore, there are very few measurements published in the literature, and only two—carried out in 1913 and 1961—are considered in the most recent critical review [2] as acceptably precise (±30 K) [3, 4]. The melting detection methods used in these experiments are, however, only qualitative (based on sample visual inspection after quenching), and the temperature measurements are not well described. Moreover, melting was produced in crucibles of tungsten, and this element was eventually found in the molten sample at concentrations of the order of 0.1%.

Perturbations were, however, also present in more recent melting-point measurements [5] obtained by laser heating, where a largely understated value of 2870 K was deduced. Some light on this difficulty was cast by the work of Petrov et al. [6, 7], who, in a detailed analysis of the thermal radiation characteristics of MgO and other translucid materials, have shown that temperature measurements by conventional pyrometers may be heavily spurious, especially if temperature gradients are present. These authors suggested that the melting temperature of MgO might fall between

3215 *and* 3230 K [8]. Now, with the pyrometric method developed in this work, the sources of errors exposed by these authors are avoided, and the reported value of the melting point ($T_m = 3250 \pm 20$ K) is in line with a realistic analysis of the radiative properties of this ceramic.

3.2. ZrO_2–UO_2

The second case examined is the melting behavior of the phase produced by chemical interaction of uranium dioxide pellets with their zircalloy cladding at a high temperature and under oxidizing conditions. The sample, basically a $(Zr,U)O_2$ mixed oxide, was obtained from the CEA reactor experiment PHEBUS, where a medium burn-up fuel assembly was submitted to a loss-of-coolant (LOCA) test. No precise melting data were available, either for the irradiated fuel or for the final reaction product. Moreover, though the ternary phase diagram of Zr–U–O has been studied since the end of the fifties, experimental data on melting are scarce and date back more than four decades [9–12]. In this work, measurements were then carried out on as-fabricated ZrO_2 as well as on $(Zr,U)O_2$ mixed oxides of selected compositions. The results were then compared to data obtained on irradiated UO_2 and on real *corium* of composition $(U_{0.6}Zr_{0.4}X)O_2$, where X is a set of minor metallic components of less than 5% concentration. The results are reported in Table I and Fig. 5.

The measurements on as-fabricated materials confirm [13] that the pseudo-binary phase diagram of UO_2–ZrO_2 exhibits a eutectic at about

Table I. Measured Melting Point and Corresponding Normal Spectral Emissivity at a Wavelength of 650 nm

Material	Type[a]	T_m (K)	ε (650 nm, T_m)
MgO	tt	3250 ± 20	0.92 ± 0.01[b]
$MgO{:}0.015AmO_2$	d	3220 ± 10	0.78 ± 0.01
$UO_{2.00}$	d	3110 ± 5	0.86 ± 0.01
$ZrO_{2.00}$	t	2950 ± 10	0.85 ± 0.01
$(U_{0.5}Zr_{0.5})O_{2.00}$	d	2805 ± 5	0.85 ± 0.01
$(U_{0.8}Zr_{0.2})O_{2.00}$	d	2926 ± 3	0.86 ± 0.005
$(U_{0.2}Zr_{0.8})O_{2.00}$	d	2810 ± 5	0.89 ± 0.01
$UO_{2.00}$:5–7 at% Zr (after a LOCA at 37,000 MWd/t)	d/irr	2950 ± 20	0.78 ± 0.02
$(U_{0.50}Zr_{0.47}Fe_{0.02}Y_{0.01})O_2$ (after a LOCA at 37,000 MWd/t)	d/irr	2760 ± 25	0.88 ± 0.03

[a] tt: translucid at room temperature and, possibly, at the melting point. t: translucid at room temperature and opaque at very high temperatures. d: dark colored. irr: reactor-irradiated sample.
[b] Effective emissivity.
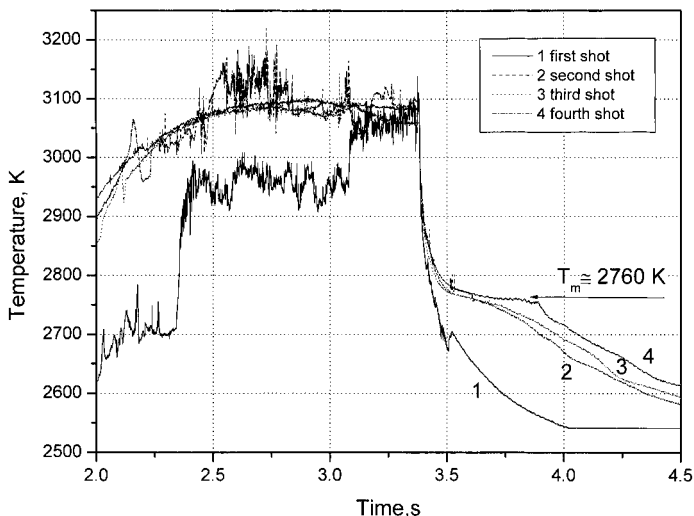
Fig. 5. Thermograms of successive pulses on irradiated corium, basically consisting of a uranium–zirconium mixed oxide. The first pulses are strongly perturbed by the release of volatile fission products and adsorbed gases.

2800 K and $U/Zr = 1.1$. At this composition, the measured thermograms *do not* exhibit the effects of a liquidus/solidus temperature gap. The composition of the liquid appears to be the same as that of the fcc solid solution. This explains the stability and the excellent reproducibility of the melting point even after repeated shots. The other solidus measurements, in mixed oxides with 20 and 80% Zr, respectively, are in agreement with the measurements of Lambertson and Mueller [9], showing an almost-constant value of the solidus temperature in the range between the eutectic composition and 80% Zr. Also, the melting point of pure zirconia (2950 ± 10 K) is within the scatter of the literature values.

Particularly interesting are the results obtained on samples of molten corium. These samples were extracted from a large lava mass, produced in the reactor core meltdown experiment PHEBUS-FPT1. The composition of the sample, measured by EDAX, is close to that of the eutectic. The melting experiments were particularly difficult since the sample contained a considerable amount of volatile impurities. In fact, during the first shot, the heat-up flank of the thermogram appears to be strongly perturbed, already at low temperatures (Fig. 5). Actually, the observed random fluctuations cannot be attributed to a variation of the surface reflectance but, rather, to emission of gas and vapors from the surface of the sample. Though the

maximum temperature reached during the laser pulse ($T_{peak} > 3500$ K) ensured the formation of a large molten pool, the perturbation of the thermal radiation continued until the laser was switched off. In the second shot, however, the heating stage was much more regular. Only after about 300 ms, at temperatures above 3000 K, did the vapor emission perturbation reappear. A stable thermal arrest in the cooling stage was detectable already in the second pulse. A sufficiently precise solidus temperature of 2760 ± 20 K was measured in the fourth pulse, i.e., about 50 K below the eutectic of the mixed oxide. This difference is likely due to the presence of iron impurities. In fact, a measurement carried out on a second sample containing approximately 10% Fe produced a markedly lower solidus temperature.

Finally, the melting point of a pellet of UO_2 irradiated up to 37,000 MWd/t and adjacent to the molten mass of corium was measured. Most of the pellet volume was still intact after the in-pile test, but the cladding and part of the fuel in contact with the molten corium were corroded away. Microprobe analysis shows that the fuel contained, in addition to fission products, approximately 8 to 20 at% zirconium coming from interaction with the molten cladding. Even in this case, vapor emission strongly perturbed the first pulse; however, in subsequent pulses, gas or aerosol emission was no longer detected, and the cooling stage exhibited regular features (Fig. 6). Analogous to molten corium, the measured melting point of
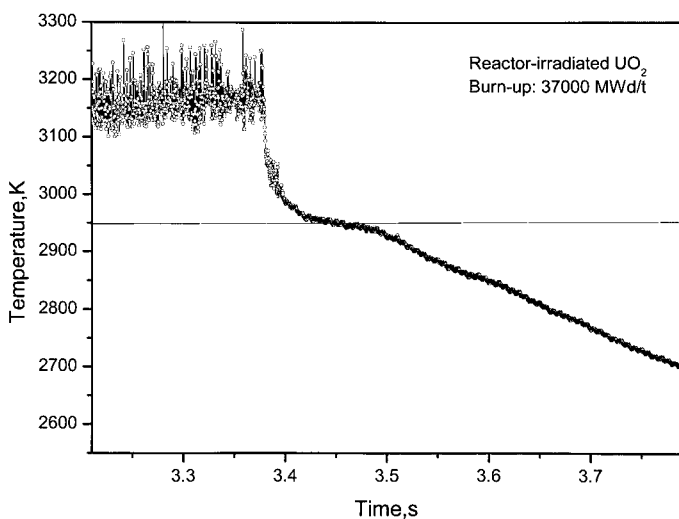
Fig. 6. Thermogram of pulse-melted UO_2 rated at 37,000 MWd/t in a light-water reactor. The material interacted with molten zircalloy and contained 5 to 7% Zr.

2950 ± 20 K is approximately 150 K lower than in the fresh fuel and only slightly lower than the solidus temperature of the mixed oxide with the corresponding Zr concentration.

4. CONCLUSIONS

(1) Melting of pure and americium-doped magnesia and zirconium–uranium mixed dioxides was produced by direct laser heating under conditions where the molten mass was mechanically stable and homogeneous in temperature. The freezing point was measured on cooling, at the temperature of the thermal arrest, which remained constant during a few tenths of seconds. Combining spectral and brightness pyrometry, the temperature was also measured with a reasonable accuracy in semitransparent materials such as MgO and ZrO_2. The measured *effective* spectral emissivity was deduced from the analysis of the thermal emission spectrum in the range of 500 to 900 nm, detected by a 200-spectral window fast spectrometer, while for opaque materials, the *real* spectral emissivity was obtained from the same type of analysis.

(2) The melting point of MgO was measured at 3250 ± 20 K, i.e., approximately 150 K higher than previously reported in the literature. This
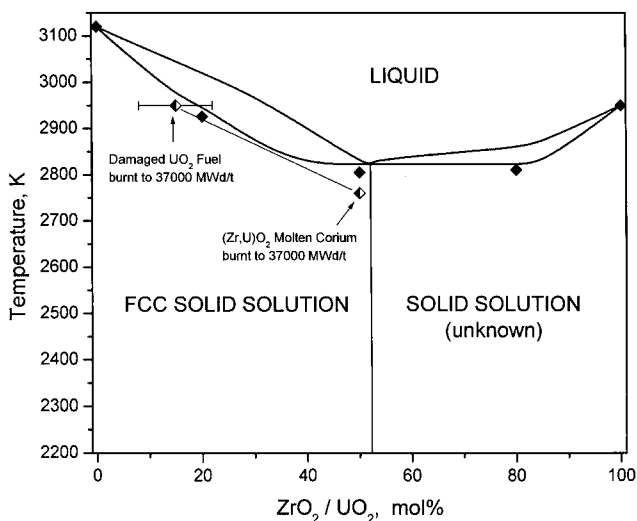
Fig. 7. Measured solidus of UO_2–ZrO_2 mixed oxides. The solid diamonds correspond to measurements on pure samples. The arrows indicate reactor-irradiated samples. The full lines correspond to the data of Lambertson and Mueller [9].

high value was confirmed by the measured melting point of $MgO:AmO_2$ (3220 ± 15 K), a dark-colored material, for which pyrometric temperature measurements are much easier.

(3) The melting point of reactor-irradiated UO_2 (37,000 MWd/t burn-up) in contact with liquid corium was measured with the same method. A significant decrease in T_m, from 3110 K, measured in the as-fabricated fuel, down to 2950 K was observed. The decrease in T_m, which remained unchanged even after repeated pulses, was due to the effect of intake of zirconium and to fission products soluble in solid UO_2.

(4) The three measured solidus temperatures of uranium–zirconium mixed oxides fell 10–20 K below the solidus line measured previously by Lambertson and Mueller [9]. One measurement of a molten corium sample at 37,000 MWd/t burn-up, with a composition near the eutectic point of the ZrO_2–UO_2 pseudo-binary phase diagram, exhibited a melting temperature only 50 K below the eutectic.

ACKNOWLEDGMENTS

REFERENCES

1. C. Ronchi, J. P. Hiernaut, and G. J. Hyland, *Metrologia* **29**:261 (1992).
2. L. V. Gurvich, I. V. Veyts, and C. B. Alcock, *Thermodynamic Properties of Individual Substance, Vol. 3* (Begell House, London, 1994), p. 397.
3. C. W. Kanolt and J. Wash, *Acad. Sci.* **3**:315 (1913).
4. R. N. McNelly, F. I. Peters, and P. H. Ribbe, *J. Am. Ceram. Soc.* **44**:491 (1961).
5. M. Bober, H. U. Karow, and K. Mueller, *High Temp. High Press.* **12**:161 (1980).
6. A. Yu. Vorobev, V. A. Petrov, V. E. Titov, and A. P. Chernyshev, *Tepl. Vys. Temp.* **30**:181 (1992).
7. A. Yu. Vorobev, V. A. Petrov, V. E. Titov, and A. P. Chernyshev, *High Temp. High Press.* **31**:227 (1999).
8. G. E. Valyano, A. Yu. Vorobev, V. A. Petrov, V. E. Titov, and A. P. Chernyshev, *Tepl. Vys. Temp.* **30**:923. (1992).
9. W. A. Lambertson and M. H. Mueller, *J. Am. Ceram. Soc.* **36**:365 (1953).
10. G. M. Wolten, *J. Am. Ceram. Soc.* **80**:4772 (1958).
11. N. V. Voronov, E. A. Voitekhova, and A. S. Danilin, *Proc. 2nd Conf. Peaceful Uses Atom. Energy, Vol. 6* (Geneva, 1958), p. 221.
12. I. Cohen and B. E. Shaner, *J. Nucl. Mater.* **9**:18 (1963).
13. K. A. Romberger, C. F. Baes, Jr., and H. H. Stone, *J. Inorg. Nucl. Chem.* **29**:1619 (1967).